

Two-colour photometric selection of high-redshift galaxies

Robin Stevens¹ & Mark Lacy^{1,2,3}

¹ Astrophysics, Department of Physics, Keble Road, Oxford, OX1 3RH. Electronic mail: rejs@astro.ox.ac.uk

² I.G.P.P., L-413 Lawrence Livermore National Laboratory, 7000 East Avenue, Livermore CA 94550

³ Dept. of Physics, University of California, Davis

31 October 2018

ABSTRACT

In this paper we describe a set of models to predict the colours of galaxies over a wide range of redshifts. We present example output from the simulations, and discuss their application to the selection of galaxies at high redshifts, particularly through identification of the Lyman break. Additionally we consider the optimal choices of filters for selection at a range of redshifts.

An interface to a subset of the simulations has been made available on the World Wide Web for the benefit of the community at the location <http://www-astro.physics.ox.ac.uk/~rejs/research/galcols.html>.

Key words: galaxies: formation – galaxies: distances and redshifts – galaxies: fundamental parameters – galaxies: photometry

1 INTRODUCTION

In recent years, two-colour selection techniques have proved themselves to be an invaluable method for identifying galaxies at high redshifts, particularly by means of choosing a filter set spanning the wavelengths between Ly α and the Lyman limit. Most notable has been the work of Steidel and collaborators (e.g. Steidel et al. 1996; Steidel et al. 1999).

As part of a project to identify radio-quiet companions to known radio galaxies in the redshift range $3 \lesssim z \lesssim 4.5$, we required theoretical models to determine the optimal selection criteria given our choice of filters. This paper discusses modelling of the expected colours for galaxies and the potential for efficiently distinguishing them from foreground stars and galaxies through broad-band photometric techniques. The results of our observations are described in a companion paper (Stevens, Lacy & Rawlings 2000).

In our searches for Lyman-break galaxies (hereafter LBGs), we initially worked to the assumptions that their spectra will be approximately flat above the rest-frame Ly α wavelength, somewhat diminished between Ly α and the Lyman limit, and have little or no flux below 912Å. Such assumptions were used for our pilot study of a region of approximately one square arcminute around the $z = 3.80$ radio galaxy 4C 41.17, described in Lacy & Rawlings (1996).

Unfortunately such naïve selection methods lend themselves to significant contamination from other red objects such as galaxies at moderate redshift (for instance where

the 4000Å break is redshifted to the position of the Lyman break at the targetted redshift) or low-mass main-sequence stars. With the benefit of the models described in this paper and of Hubble Space Telescope images of the region studied in our pilot study, which have subsequently been made available through the HST Archive, we conclude that the majority of the high-redshift candidates previously identified are in fact foreground contaminants.

For more efficient selection, a much more detailed analysis will be required and the following points must be considered within the models:

- (i) Intrinsic spectra of starbursts
- (ii) Attenuation due to intergalactic HI absorption systems
- (iii) Effects of dust extinction
- (iv) Broad-band colours and potential for confusion with other objects through photometric selection techniques
- (v) Apparent magnitudes of high-redshift star-forming galaxies for particular cosmologies, likely star-formation rates and consequences for their observability

Throughout this paper, we follow the convention established by Steidel et al. (Steidel & Hamilton 1992) of using the AB magnitude system of (Oke & Gunn 1983), conversions for which are given in Table 1. This has the great advantage of being a magnitude system in which the colours of an unreddened star-forming galaxy between bandpasses sampling the rest-frame ultraviolet continuum will be close to zero.

* Present address: Oxford University Computing Services, 13 Banbury Road, Oxford, OX2 6NN

Filter	λ_{eff} (Å)	m_{AB} (Vega)
<i>U</i>	3664	0.780
<i>B</i>	4394	-0.105
<i>G</i>	4869	-0.098
<i>V</i>	5449	0.000
<i>R</i>	6396	0.186
<i>I</i>	8032	0.444

Table 1. Conversions between AB and Vega-based magnitudes of the principal filters used in our models.

1.1 Previous work

Guhathakurta and co-workers (Guhathakurta, Tyson & Majewski 1990) searched for LBGs in relatively deep *UB_JRI* images, but were unable to provide followup spectroscopic evidence. They estimated the strength of the break at the Lyman limit from consideration of the UV spectra of O and B stars, with synthetic spectra showing breaks of a factor in the range 2–5 for a wide variety of input initial mass functions (IMFs), even without considering interstellar or intergalactic absorption by neutral hydrogen. Candidate LBGs are selected from their $U - B_J$ and $B_J - I$ colours. Their resulting selection region is somewhat conservative compared to later work, as it does not take into account the possibility of a substantial drop in flux below Ly α .

Most of the work of Steidel and collaborators makes use of a non-standard filter system, originally chosen for its suitability to a field containing a QSO and damped Lyman α system at known redshifts (Steidel & Hamilton 1992). Initially, selection is done taking into account intergalactic absorption measurements from QSO spectra (Sargent, Steidel & Boksenberg 1989), while later selection criteria are revised to take into account the detailed analysis of intergalactic attenuation by Madau (1995), which we use ourselves in § 3. Subsequent spectroscopic observations show that the selection process is highly effective with less conservative selection criteria. The lower bound in $U_n - G$ has been relaxed from 1.5 to 1.0, with a resulting increase in surface density (to the magnitude limit of $\mathcal{R} < 25.0$) from around 0.5 candidate objects per arcmin² to around 1.25 per arcmin² (Steidel et al. 1997; Adelberger, Steidel et al. 1998).

Madau et al. (1996) use a similar approach to that described here in order to determine appropriate regions in two-colour space for the selection of U_{300} and B_{450} dropouts in the northern HDF. We develop this approach to a wider range of filters, including those typical of those found on ground-based optical CCD and NIR cameras, and to span as wide a range of potential galaxy scenarios as possible.

2 SIMULATED BROAD-BAND COLOURS OF GALAXIES

In order to devise efficient selection criteria for high-redshift galaxies, it is necessary to model the expected colours of a wide variety of different types of galaxies for all redshifts at which one might possibly expect to be able to see objects.

We base our models on the PÉGASE code of Fioc & Rocca-Volmerange (1997) (hereafter FRV); our thanks go

to them for making the code publicly available. [†] The FRV code produces synthetic galaxy spectra to a resolution of 10Å from 220–8780Å in the rest-frame[‡], and to 200Å in the NIR. Like most current techniques for modelling the integrated spectrum of a population of stars, the FRV code uses the isochrone technique (Bruzual & Charlot 1991). A library of higher-resolution spectra is available, but this only covers the rest frame optical and is thus of little use when the objects are redshifted; besides which the higher resolution data is not overly crucial when dealing with broad bandpasses.

A substantial library of synthetic galaxy spectra using a wide variety of different input parameters to the FRV code was built up.

2.1 Variations of input parameters

2.1.1 Evolutionary tracks

Two sets of stellar evolutionary tracks are made available with the FRV code, namely “Padova” (Bressan et al. 1993) and “Geneva” (Schaller et al. 1992; Charbonnel et al. 1996). Post main sequence evolution, in particular that along the asymptotic giant branch for the most massive stars (Jimenez et al. 1999), proves the most difficult phase to trace in such tracks. Primarily this affects the NIR luminosity, with only a slight effect in the UV.

Another limitation is that the evolutionary tracks used are for solar metallicity, and will therefore not be an accurate representation of those in metal-poor regions such as may be found in the early universe. The version 2.0 FRV code attempts to redress this problem (Fioc & Rocca-Volmerange 2000), and will be incorporated into our models at a future date. Early indications are that metallicity significantly affects the slope of the UV continuum, with bluer spectra at low metallicities. Evidently this will have a considerable effect upon the derived star formation rates. Further work with the new models is required to investigate this more thoroughly.

2.1.2 Initial Mass Function

The FRV code by default incorporates the IMFs of Salpeter (1955), Scalo (1986), Miller & Scalo (1979) and of Kroupa (Kroupa, Tout & Gilmore 1993). The Salpeter is the simplest and still in widespread usage, but somewhat in error at the extremes. Later IMF models are an improvement in this respect, being somewhat more realistic and with less abrupt cut-offs at both ends, but are still limited by the the ability to observe the full range of stellar masses only in the solar neighbourhood.

The Kroupa IMF results from work on stars in the galactic disk which resolves the apparent differences between observations made in the solar neighbourhood and those derived from surveys to much greater distances. It is probably

[†] A more recent version of the code has recently been announced (Fioc & Rocca-Volmerange 2000), but at present our models are built around the version one code.

[‡] This resolution was higher than that of the Bruzual-Charlot models available at the time (Bruzual & Charlot 1993), an important factor when one wishes to shift the spectra to high redshifts.

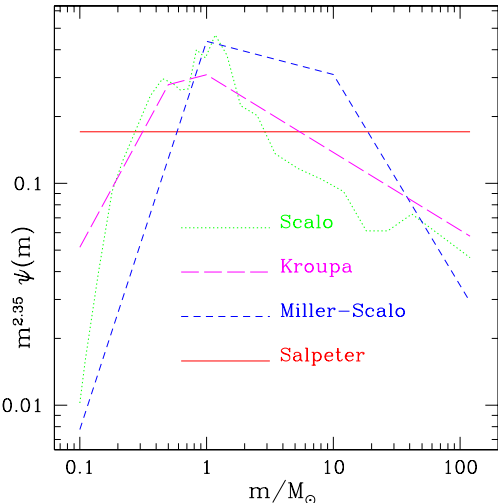


Figure 1.

Representations of the four initial mass functions used in the simulations. For clarity, all have been multiplied up by a factor $m^{2.35}$; this gives a constant slope for the Salpeter IMF.

to date the most realistic representation of the IMF in our own galaxy and it is used as the default in our models.

Applying such empirically-derived IMFs to star-formation in the early universe is a big assumption, given our limited understanding of the physical processes involved. For example, low metallicity, different cloud dynamics and the possible influence of AGN activity upon star-formation may all affect the high-redshift IMF.

The high-mass slope of the IMF is of particular interest to us since it determines the numbers of O and B stars which dominate the UV luminosity in star-forming galaxies. Any estimate of star-formation rate based on the UV luminosity is thus strongly dependent on the choice of IMF. For simplicity and ease of comparison, star formation rates are generally derived for a Salpeter IMF, but one must bear in mind that with, for example, a Kroupa IMF as opposed to a Salpeter distribution, the overall star-formation rate may be a factor of ~ 2 higher if derived from the UV luminosity. The effects of extinction due to dust will boost the SFR higher still.

2.1.3 Nebular emission

FRV use a default value for the fractional Lyman continuum absorption $f = 0.7$, in agreement with LMC HII values (DeGioia-Eastwood 1992), but for completeness values from 0 to 1 were considered. This would have considerable effect on the strength of the Lyman break save for the fact that intergalactic attenuation becomes the dominant effect at redshifts sufficiently high for us to observe below the Lyman limit (§ 3). However it does govern the strength of emission lines, which, particularly in the case of Ly α , can in principle have considerable effect on the observed colours, though it is often strongly suppressed. Continuum emission is increased in the rest-frame optical, but this will only have an effect on the infrared colours of galaxies at high redshift.

2.2 Star-formation model

A variety of star-formation models are included in the FRV code, ranging from instantaneous bursts to constant SFR scenarios. Primarily the choice affects how quickly the galaxy spectrum evolves from that of young starbursting regions to that of aged ellipticals. We include in the final models galaxy spectra covering a very wide range of star-formation models and ages, subject to a conservative cut-off to eliminate galaxies at ages unphysical for any reasonable cosmology given their redshift. Thus the models include more or less any conceivable galaxy type.

2.3 Other parameters

The models also incorporate variations of initial star formation rate, governing the timescale over which stars are formed, and the fraction of stellar ejecta available for further star formation. This latter only affects galaxies sufficiently aged for a substantial proportion of the stars originally formed to go through the late stages of stellar evolution; significant star formation resulting from stellar ejecta results in the overall galaxy spectrum being a combination of the UV spectrum of a young star-forming galaxy together with the optical and NIR spectrum expected of an aged galaxy.

Dust extinction is also considered, but rather than use the FRV extinction routine, we chose to use our own as described in § 4.

The spectra were then convolved with selected broadband filter profiles (those of the WHT optical and NIR filter sets, and the HST WFPC2 filters as used in the HDF observations), scaled to the luminosity of a galaxy of stellar mass $10^{10} M_\odot$, and the AB magnitudes output.

3 INTERGALACTIC ATTENUATION BY THE LYMAN- α FOREST AND BY LYMAN LIMIT SYSTEMS

To approximate intergalactic attenuation, the method of Madau (1995) was followed. Equations 12 and 13 of his paper were used to correct for the Lyman- α forest. To correct for absorption of the Lyman continuum we made use of the approximate numerical integration of his Equation 16, which he states is good to 5%. For our purposes this is perfectly adequate and computationally inexpensive.

Given the random distribution of the absorbers, significant deviations from the mean attenuation are to be expected at any particular wavelength. In the Lyman- α forest region, this does not present any problem, since the use of broad bandpasses means that one will be averaging over a large number of absorbers.

Madau's figure 2 shows the measured flux decrements for quasar spectra within bandpasses of $\sim 100\text{\AA}$ in the rest-frame. Few decrements differ from the estimated mean by more than about 0.1 mag. In our case we can expect an even greater averaging effect to act in our favour owing to the wider bandpass of our filters.

Below the Lyman limit, a substantial contribution to the attenuation will come from the much rarer Lyman limit systems (LLS), for which the mean number along any line

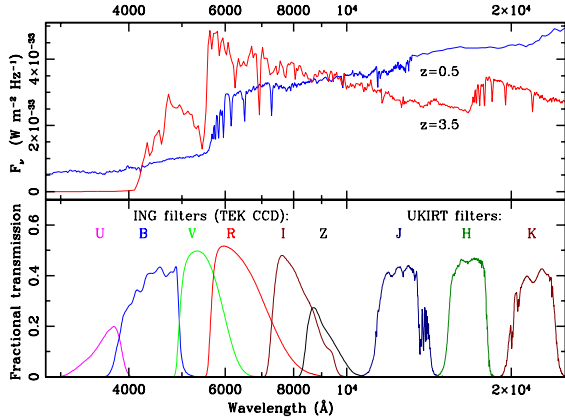


Figure 2.

Model spectra in f_ν for a $z = 3.5$ galaxy undergoing star formation at a constant rate of $10M_\odot \text{ yr}^{-1}$, and for an evolved galaxy at $z = 0.5$, typical of lower-redshift galaxies likely to have similar colours to the targeted high-redshift objects owing to the presence of the 4000Å break. Our selection criteria must therefore be able to discriminate effectively between the two, using the much bluer continuum colour of the high-redshift object relative to the low-redshift galaxy. The Lyman- α and Lyman-limit breaks are clearly visible in the former; similar objects may possibly pass the selection criteria for both U and B dropouts.

Also shown are the response curves for various filters. The optical filters are those from the Isaac Newton Group telescopes on La Palma and include those used in our observations (a similar set of filters plus the Z is being used for the wide field survey of Dalton et al. currently in progress at the INT); all filter profiles have been convolved with the response curve for the TEK CCD used in our observations. The JHK filter profiles are taken from data available on the UKIRT WWW pages.

No scan was available for the G filter (loaned by Richard McMahon); for these models a bandpass of width 1000Å centred at 4900Å has been assumed, as per the design specifications.

of sight will be of order unity. There is, however, a significant probability that there will not be a single LLS along a particular line of sight, about 10% at the redshifts of interest. While in the case of the Ly α forest, the distribution of the number densities of absorbers about the mean can be approximated by a Gaussian at the redshift of interest, such an approximation cannot be made for the LLS.

The chances of an object missing our selection cuts owing to the absence of a LLS along the line of sight are greater for U dropouts than for B dropouts for two reasons. Firstly, the relative contribution of the LLS to the attenuation at $z \sim 3$ is greater than at $z \sim 4$ (see Figure 3). Secondly, the expected number of LLS along a line of sight increases significantly between $z \sim 3$ and $z \sim 4$.

Møller & Jakobsen (1990) give values ranging from 0.25 at $z_e = 2.5$ to about 0.05 at $z_e = 4.5$ for the probability of encountering no LLS leading to an absorption depth $\tau > \tau_{crit} = 1.5$ at the HeII line $\lambda_e = 304\text{\AA}$. As the photoionisation cross-section of H decreases approximately as ν^{-3} below the Lyman limit, this optical depth corresponds to a very optically-thick Lyman limit system, but these probabilities are a useful indicator of how the likelihood of encountering a Lyman limit system changes with redshift.

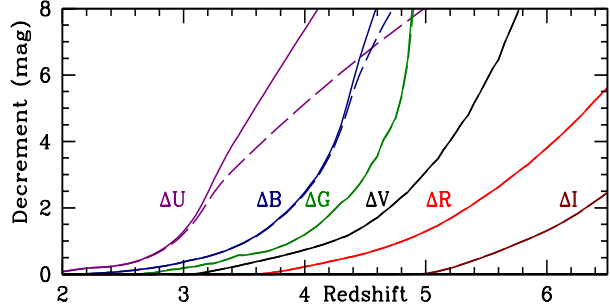


Figure 3.

Variation of magnitude decrements with redshift for the six broadband filters used in our own observations. Solid lines show the mean decrement due to *all* absorbers, while dashed lines do not include the contribution of Lyman limit systems. Note in particular that the absence of LLS absorbers along a particular line of sight is most likely to affect the chances of detecting U dropouts at redshifts $3 \lesssim z \lesssim 3.5$. Even so, a substantial break should be observed even without a LLS absorber on the line of sight.

4 DUST EXTINCTION

While in the optical a measure of the dust extinction is obtainable from the emission line Balmer optical depth τ_B^l , dust extinction in the UV is typically parametrized in terms of the continuum slope. The UV continuum of a star-forming galaxy may be approximated by a power law $F(\lambda) \propto \lambda^\beta$, with a ‘‘colour excess’’ defined by $E(\beta) = \beta - \beta_0$. Spectral synthesis models give a value $-2.5 \lesssim \beta_0 \lesssim -2.0$, in broad agreement with measured values. For a young stellar population (age $\lesssim 2 \times 10^7$ yr), the differences, other than of normalisation, between the spectra of the extreme scenarios of instantaneous burst and constant star formation rate are small and within measurement uncertainties.

We calculate dust extinction according to the method of Calzetti, Kinney & Storchi-Bergmann (1994, hereafter C94), taking the extinction parameter $A(\lambda)$ to be empirically fitted by a third-order polynomial $Q_e(x)$ (where $x = 1/\lambda$ such that $A(\lambda) = \tau_B^l Q_e(x)$).

Q_e is purely the *selective* extinction as opposed to the *total* extinction, since for any spectral slope β one does not in general know at what wavelength there is *no* extinction. To obtain the total extinction, we use the method described by Meurer et al. (1995), using consideration of energy conservation (relating the far IR excess to β). The ratio of total to selective extinction is parametrized as $X'_\lambda = A_\lambda/E(\beta)$. For the HST F220W filter (central wavelength 2280Å, thus $Q_e(F220W) = 1.582$) and the C94 starbursts, this value is constant at $X'_{F220W} = 1.6$.

Using the starburst values of C94 to give $\tau_B^l = 0.494E(\beta)$ and choosing $\beta_0 = -2.5$, we obtain

$$f'(\lambda) = \frac{10^{-0.4 \times 1.6(\beta+2.5)} f(\lambda)}{\exp[0.494(\beta+2.5)(Q_e(\lambda) - 1.582)]} \quad (1)$$

The dust extinction corrections are applied to our synthetic spectra prior to correcting for intergalactic extinction, using values for β of -2.5 (zero extinction), -1.5 and -0.5 (equivalent to $E(B-V)$ of 0.00, 0.23 and 0.46).

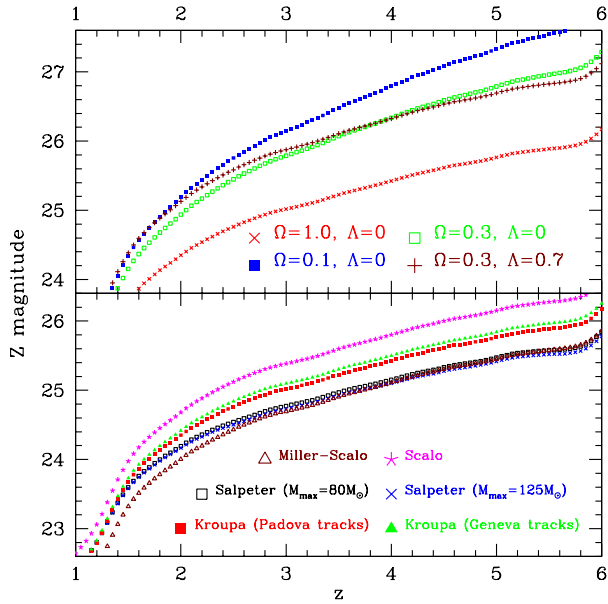


Figure 4.

Variation of Z magnitude with redshift for an unreddened star-forming galaxy with a continuous star formation rate of $10 h_{50}^{-2} M_{\odot} \text{ yr}^{-1}$. The top plot shows the effect of changes in cosmology for a Kroupa IMF. The bottom plot shows the effect of varying the initial mass function for $\Omega = 1$, $\Lambda = 0$ and Padova evolutionary tracks except where indicated. Sensitivity to the choice of evolutionary track is at the 5% level (though this is likely to increase if metallicity effects are taken into account), but the choice of IMF has a very significant effect on the luminosity-SFR calibration. Z is used as Ly α does not reach the band until $z \approx 5.8$, and hence it represents the unattenuated UV continuum flux. While the unreddened UV continuum is frequently regarded as a flat spectrum, this is merely an approximation, and K correction effects lead to the variation of magnitude with redshift differing slightly from the distance modulus.

5 LUMINOSITY-SFR CALIBRATION

For the calibration between observed magnitude and star-formation rate, we choose for ease of comparison to use the same model as Steidel et al. (1996), namely a Salpeter IMF with upper mass cutoff at $80M_{\odot}$ — this low cutoff has a significant effect on the magnitude (Figure 4).

For an $\Omega = 1$, $\Lambda = 0$ cosmology with $H_0 = 50 \text{ km s}^{-1} \text{ Mpc}^{-1}$, we find that a constant star formation rate of $10.0M_{\odot} \text{ yr}^{-1}$ with solar metallicity at $z = 3.25$ corresponds to a magnitude in R of 24.88 at age 100Myr, tending asymptotically to $R = 24.79$ as the galaxy ages[§]. This is slightly fainter than the value quoted by Steidel et al., but probably insignificant in view of the use of different spectral synthesis codes and stellar libraries.

Figure 4 shows the effect of changes in IMF, cosmology and evolutionary tracks. It is evident that accurate determination of the shape of the Madau curve is dependent on the cosmology, initial mass function and more accurate representations of stellar evolution at low metallicities.

[§] By an age of 60Myr, the luminosity is within 10% of this figure, and within 1% by an age of 400Myr.

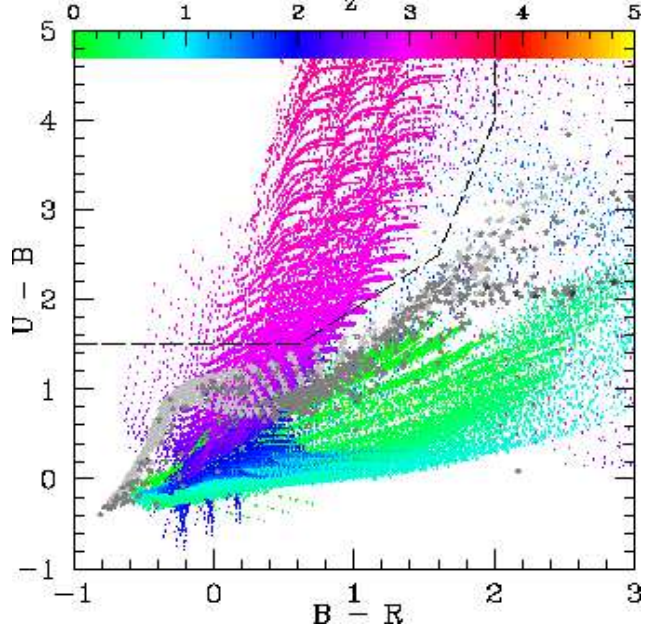


Figure 5.

Variation of $U - B$ and $B - R$ colours with redshift z . Galaxies are indicated by small dots coloured by redshift; young (age $< 100 \text{ Myr}$) galaxies in the redshift range $2.75 < z < 3.5$ have been emphasized. The colours of galactic stars have been superimposed: light grey stars are those from the model data of Bessel, Castelli & Plez (1998), while the darker grey stars are from the photometric standards of Landolt (1992). Black stars represent M dwarfs and use data obtained from Bessell (1991) and Leggett (1992).

Our selection criteria are indicated by the dashed lines. A broad area of colour-colour space is enclosed, allowing for efficient selection of candidate high-redshift galaxies in spite of photometric errors, as long as a sufficiently large break in $U - B$ can be observed. In practice this is the limiting factor, owing to the relatively poor quantum efficiency U of the TEK CCDs used compared to that of more modern detectors.

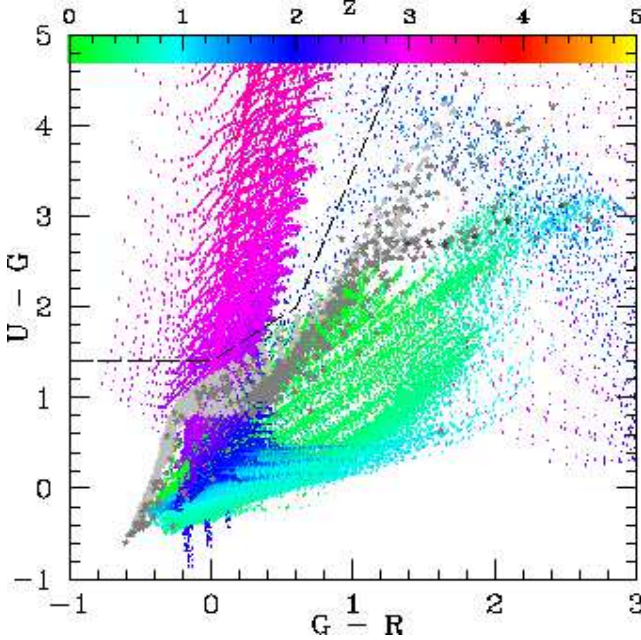
Galaxies at redshifts above $z \approx 3.5$ will have almost complete absorption in U and thus extreme $U - B$ colours off the top of this plot, but in practice we will only measure lower limits to this colour. As redshift increases, increasing absorption in B will push $B - R$ further towards the red. Making the upper bound to the cut in $B - R$ (or more generally for the two longer wavelength bandpasses) further to the red allows for selection of objects at higher redshifts than are shown on this plot, however this must not be pushed so far as to reach the stellar locus.

6 MODEL COLOUR-COLOUR PLOTS

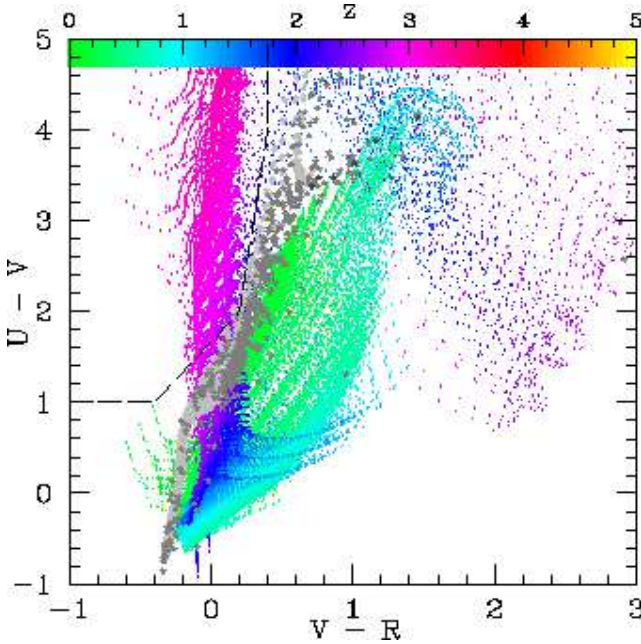
Colour-colour plots for some of the three-filter photometric systems used in our observations are presented in Figures 5 to 10. A wider range of plots is available via the WWW at our website (Stevens 1999a), together with an interface for the generation of plots for arbitrary colour pairs within a substantial database of optical, NIR and HST filters.

Galaxy colours are plotted at redshift increments of 0.05, together with colours typical of galactic stars, and our chosen selection criteria are shown. Young galaxies within the targetted redshift ranges have been highlighted for clarity.

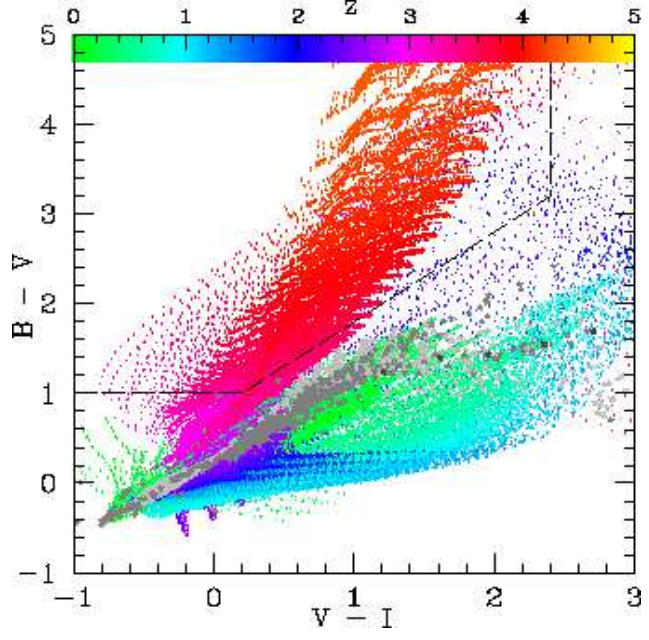
In producing these plots, no assumptions have been

**Figure 6.**

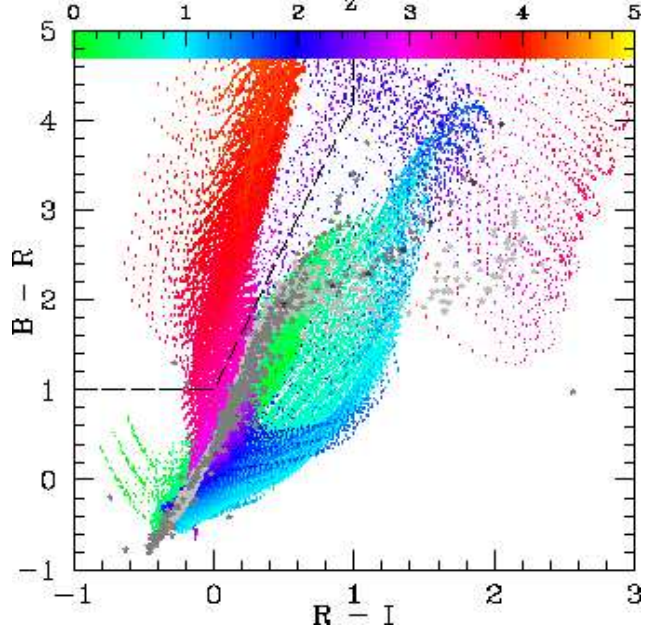
As Figure 5 but for $U - G$ and $G - R$. G magnitudes for stars are derived by interpolation from the B and V magnitudes. Note in particular the decrease in the area of colour-colour space in the selection area relative to Figure 5.

**Figure 7.**

As Figure 5 but for $U - V$ and $V - R$. The low $V - R$ colours for stars and low-redshift galaxies mean that the colour must be tightly constrained to avoid severe problems with contamination of candidate high-redshift objects and use of these colours to select high-redshift galaxies therefore not recommended. However it may provide a useful check in deep multicolour surveys.

**Figure 8.**

As Figure 5 but for $B - V$ and $V - I$, and with galaxies in the redshift range $3.5 < z < 4.5$ emphasized. Again there is good separation between the high-redshift galaxy population and the low redshift galaxies and stars.

**Figure 9.**

As Figure 8 but for $B - R$ and $R - I$. In comparison with the BVI method (Figure 8), the separation between the high-redshift galaxies and the stars and low redshift galaxies is poor, making efficient selection harder without good limits on the $B - R$ colour.

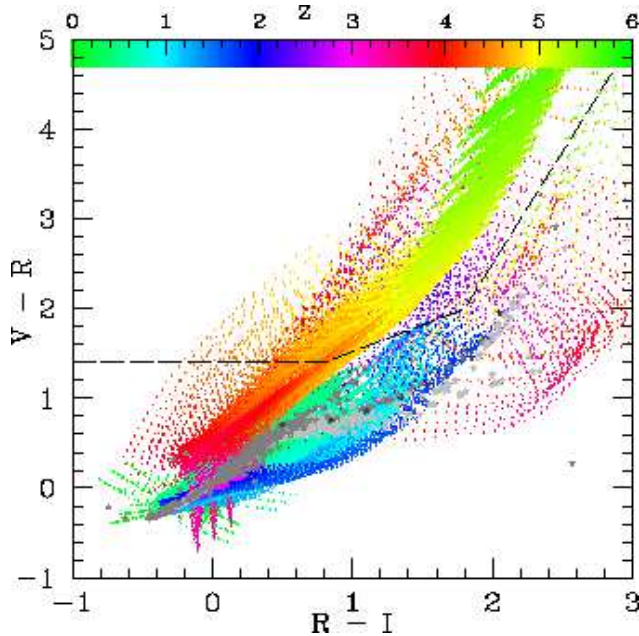


Figure 10.

As Figure 9 but for $V - R$ and $R - I$. Selection of candidates at $z \sim 5$ is perfectly feasible, but spectroscopic confirmation of objects becomes increasingly difficult as the redshift increases.

made as to whether objects are likely to be observable. Galaxies are shown at all redshift intervals for which the ages of the oldest stars are less than the age of the Universe in any reasonable cosmology. In some cases evolved high-redshift objects will therefore be shown which are unphysically old or at least exceedingly unlikely to be observable within the foreseeable future.

Such plots can be used to determine the most effective use of broad-band filters to detect Lyman-break objects in future surveys. For efficient selection one must try to separate the locus of Lyman-break objects as much as possible from that of stars and low-redshift galaxies, an important factor is thus to ensure a reasonable span in wavelength between the filters used for selection. Figure 7 clearly shows the problem in using V and R as the two longer-wavelength bandpasses, since the two are too close in effective wavelength to give a significant colour term on intrinsically red objects. Using G as the central filter is better (Figure 6) but Figure 5 shows that B is optimum.

Obviously the choice of filters will be influenced somewhat by the targeted redshift, three-filter selection working most effectively where the central filter spans the wavelength of redshifted Ly α . UBR will be ineffective at selection of objects much beyond $z \approx 3.1$, whereas Steidel and co-workers have already shown the effectiveness of a system similar to our UGR out to around $z \approx 3.5$. Again, UGR is inappropriate beyond this: for instance we note that the radio galaxy 4C 41.17 at $z = 3.80$ is too red in $G - R$ to be selected in UGR , but is a clear dropout in $UVRI$.

When searching for objects beyond $z \approx 3.5$, it becomes preferable to use B rather than U as the shortest wavelength bandpass. While $UVRI$ selection would in principle work well, the increased observing time required to make sufficiently

deep observations in I rather than R owing to the increased sky background makes it advantageous to use B in place of U to decrease the necessary observing time in the bluest filter. As a central wavelength, V is preferable to R owing to the greater separation between high-redshift galaxies and low redshift objects, as can be seen from Figures 8 and 9.

7 EXTENSIONS TO $Z > 4.5$

Selection of candidates at redshifts beyond $z \sim 4.5$ is perfectly feasible given sufficiently deep observations, although spectroscopic confirmation of such objects becomes much more difficult due to absorption and emission lines becoming redshifted to among the OH bands of the near-IR.

Steidel's group have added an I filter to their U_nGR system in order to look for G dropouts at $z \sim 4.5$, and have had considerable success (Steidel et al. 1999). At higher redshifts still, V dropouts can be searched for. A VRZ filter system is in theory very effective at selecting galaxies at $z \sim 5$, but observational considerations will in general make this impractical owing to the very high sky background, poor sensitivity of CCDs and severe problems with fringing if thinned CCDs are used.

In practice VRI is likely to be more suitable, indeed we use the data obtained in one of our fields to conduct a pilot study, but conclude that our data are insufficiently deep to probe a population of V dropouts at $z \sim 5$. Z imaging could be more effective with the use of large-format infra-red arrays, which are a factor of ~ 2 more sensitive than CCDs at such wavelengths, but the much greater area of CCDs, particularly in the form of large mosaic cameras, will give them the edge for some time to come.

Deep multicolour imaging surveys using large-format detectors will reveal many candidates. One such survey is being undertaken by researchers at Oxford using the Wide Field Camera on the Isaac Newton Telescope, imaging ten square degrees in $BVRI$ to depths comparable with this work, with subareas also imaged in U and Z . Among the many possibilities of these data is that of searching for bright Lyman-break galaxies spanning the range $2.8 \lesssim z \lesssim 5$. Given the detection limits of the survey, we expect to find ~ 15000 U dropouts at $z \sim 3$, 2000 or more R dropouts at $z \sim 4$ and ~ 100 V dropouts at $z \sim 5$ (Stevens 1999b).

Shallower surveys can still make use of similar techniques for finding high-redshift objects. Though insufficiently deep to find galaxies at such redshifts, the Sloan Digital Sky Survey will probe quasars and other bright active galactic nuclei. Very similar colour selection techniques to ours have been applied to commissioning data to identify candidate quasars at redshifts above $z \gtrsim 3.6$ (Fan et al. 1999; Fan et al. 2000).

Beyond $z \sim 6$, intergalactic attenuation will affect even Z band and objects at $z > 6$ with star-formation rates typical of objects at $z \sim 3$ will have NIR magnitudes of 26 or beyond, difficult to observe even with long observations on 8–10m class telescopes. Ultimately observations of the earliest star-formation in the Universe at $10 \lesssim z \lesssim 30$ must be the preserve of NGST and similar instruments.

Field	z	Filter choice	
		Ideal	of <i>UBVRIZ</i>
?	$\gtrsim 5.3$	$r'i'z'$	<i>RIZ</i>
TN J0924-2201	5.19	<i>VRI</i>	<i>VRI</i>
6C 0140+326	4.41	<i>GRI</i>	<i>BVI</i>
8C 1435+635	4.25	<i>GRI</i>	<i>BVI</i>
4C 41.17	3.80	<i>BVI</i>	<i>BVI</i>
6C 0032+412	3.65	<i>BVI</i>	<i>BVI</i>
B2 0902+343	3.40	<i>UGR</i>	<i>UBR</i>
	$\lesssim 3.0$	$u'GR$	<i>UBR</i>

Table 2. Choice of filters for searching for galaxies at similar redshift to the central radio galaxy in various high-redshift radio galaxy fields, including those targeted in our own work (Stevens, Lacy & Rawlings 2000). $u'g'r'i'z'$ refer to the SDSS filter set. At $z \lesssim 3$ a filter slightly bluer than the standard *U* filter such as u' or the U_n of Steidel et al. will give a sharper break below Ly α , while the lesser overlap between the filters of the Sloan set are more suitable when searching for *R* dropouts. Inevitably the choice depends on the availability of filters for a particular instrument, but in many cases use of a customized filter set, with minimal overlap between filter bandpasses, will provide greater efficiency at a particular target redshift. In particular we conclude that such techniques are likely to perform very poorly for target redshifts $4 \lesssim z \lesssim 4.7$ if one is restricted to a standard set without a *G* or similar filter between *B* and *V*.

8 ACKNOWLEDGEMENTS

We thank Steve Rawlings, Lance Miller, Max Pettini, Gavin Dalton and Tony Lynas-Gray for helpful discussions. REJS acknowledges the support of a PPARC studentship. This research has made use of NASA's Astrophysics Data System Abstract Service.

REFERENCES

Adelberger K. L., Steidel C. C. et al., 1998. *ApJ*, 505, 18.
 Bessel M. S., Castelli F., Plez B., 1998. *AA*, 33, 231.
 Bessel M. S., 1991. *AJ*, 101, 662.
 Bressan A. et al., 1993. *AAS*, 100, 647.
 Bruzual G., Charlot S., 1991. *ApJ*, 367, 126.
 Bruzual G., Charlot S., 1993. *ApJ*, 405, 538.
 Calzetti D., Kinney A. L., Storchi-Bergmann T., 1994. *ApJ*, 429, 582.
 Charbonnel C. et al., 1996. *AAS*, 115, 339.
 DeGioia-Eastwood K., 1992. *ApJ*, 397, 542.
 Fan X. et al., 1999. *AJ*, 118, 1.
 Fan X. et al., 2000. *AJ*, in press, preprint no. astro-ph/0005414.
 Fioc M., Rocca-Volmerange B., 1997. *AA*, 326, 950.
 Fioc M., Rocca-Volmerange B., 2000. *in preparation*, preprint no. astro-ph/9912179.
 Guhathakurta P., Tyson J. A., Majewski S. R., 1990. *ApJ*, 357, L9.
 Jimenez R. et al., 1999. *MNRAS*, in press.
 Kroupa P., Tout C. A., Gilmore G., 1993. *MNRAS*, 262, 545.
 Lacy M. D., Rawlings S., 1996. *MNRAS*, 280, 888.
 Landolt A. U., 1992. *AJ*, 104, 340.
 Leggett S. K., 1992. *ApJS*, 82, 351.
 Madau P. et al., 1996. *MNRAS*, 283, 1388.
 Madau P., 1995. *ApJ*, 441, 18.
 Meurer G. R. et al., 1995. *AJ*, 110, 2665.
 Miller G. E., Scalo J. M., 1979. *ApJS*, 41, 513.
 Møller P., Jakobsen P., 1990. *AA*, 228, 299.
 Oke J. B., Gunn J. E., 1983. *AA*, 266, 713.
 Salpeter E. E., 1955. *ApJ*, 121, 161.
 Sargent W. L. W., Steidel C. C., Boksenberg A., 1989. *ApJS*, 69, 703.
 Scalo J. M., 1986. *Fund. Cosm. Phys.*, 11.
 Schaller G. et al., 1992. *AAS*, 96, 269.
 Steidel C. C., Hamilton D., 1992. *AJ*, 104, 941.
 Steidel C. C. et al., 1997. In: *The Young Universe, Rome Observatory*, p. 428, eds D'Odorico S., Fontana A., Giallongo E.
 Steidel C. C. et al., 1996. *ApJ*, 462, L17.
 Steidel C. C. et al., 1999. *ApJ*, 519, 1.
 Stevens R. E. J., 1999a.
<http://www-astro.physics.ox.ac.uk/~rejs/research/>,
Searches for High-Redshift Galaxies. University of Oxford.
 Stevens R. E. J., 1999b. *DPhil thesis*, University of Oxford.
<http://www-astro.physics.ox.ac.uk/~rejs/research/thesis/>.
 Stevens R. E. J., Lacy M. D., Rawlings S., 2000. *MNRAS*, in preparation.

This paper has been produced using the Royal Astronomical Society/Blackwell Science L^AT_EX style file.